Response of saturated porous media to cyclic thermal loading

Eric Blond, Nicolas Schmitt, François Hild

MECHANICS OF COHESIVE-FRICTIONAL MATERIALS
Mech. Cohes.-Frict. Mater. 2000; **00**:1–12 *Prepared using* cfmauth.cls *[Version: 2000/03/22 v1.0]*

Response of saturated porous media to cyclic thermal loading

E. Blond *, N. Schmitt and F. Hild

LMT-Cachan
(E.N.S. de Cachan / C.N.R.S U.M.R. 8535 / University Paris 6)
61 avenue du Président Wilson, F-94235 Cachan Cedex, France

SUMMARY

The response of a semi-infinite saturated porous medium submitted to a harmonic thermal loading on its free face is studied herein. The pressure diffusion equation that governs the fluctuation of the interstitial pressure is established. This equation allows us to obtain prevalent parameters. The location of the maximum fluid pressure is derived and it is shown to depend on the diffusivity ratio and the frequency of the thermal loading. Furthermore, it is also established that the maximum fluid pressure depends on the diffusivity ratio and the thermal amplitude only. Copyright © 2000 John Wiley & Sons, Ltd.

KEY WORDS: Porous Media; Heat transfer; Harmonic loading; Maximum interstitial pressure

1. INTRODUCTION

Poromechanics is widely used in various applications where both the fluid mass transfer and the mechanical behavior must be modeled, from biomechanics to material sciences [1]. This work deals with the thermomechanical behavior of saturated porous media. The estimation of the response of porous media subjected to thermal loading is of interest in various engineering fields such as extraction of oil [2], concrete resistance against fire [3], reliability of airfield [4], nuclear waste disposal [5], experimental measurement of low permeability [6]. The reliability of the working lining of steel ladles is yet another case for which the above-mentioned framework can be applied [7].

In steel ladles, the inner layer of a composite refractory lining is in contact with molten slag during casting. Bauxite bricks used for this wear layer are impregnated by slag over a few centimeters. In the wetted area, microcracks appear, propagate parallel to the hot face during the following casting and cause spalling [7]. In this problem, strong couplings exist between heat transfer due to the cyclic thermal loading varying between 1200^oC and 1600^oC, deformation of the porous matrix due to structural and material effects, fluid mass flow (i.e., liquid slag), chemical reactions (e.g., dissolution, precipitation) and phase transformations.

*Correspondence to: E Blond, LMT-Cachan, E.N.S. de Cachan, 61 avenue du président Wilson, F-94235 Cachan, France, Tel: +33 1 47 40 22 55, Fax: +33 1 47 40 22 40, E-mail: blond@lmt.ens-cachan.fr

Received ??
Revised ??
!

The aim of this work is to investigate the role played by the liquid slag in the initiation of spalling. One cause that could be responsible for crack initiation is that the molten slag present in the refractory open porosity (typically $15-20\%$) produces an interstitial pressure that is high enough to induce additional tensile stresses in the refractory brick. Consequently, the thermomechanical coupling between liquid mass transfer and the deformation of the solid skeleton will be studied herein.

The first development of a poromechanical approach for an elastic and isotropic porous medium under isothermal condition was proposed by Biot [8]. This work was generalized for anisotropic elastic media [9] and for viscoelastic porous media [10]. Rice and Cleary [11] recast Biot's theory in terms of easier physical interpretations and developed general methods of resolution. They have also underlined that considering the stress tensor and pore pressure as basic variables may be advantageous to the Navier formulation.

Different approaches have been proposed to develop an anisothermal theory. For example, Derski and Kowalski [12] derived from the thermodynamics of irreversible processes a complete set of equations that accounts for the thermal effects. Palciauskas and Domenico [13] extended Biot's theory with some anisothermal modifications. They established an upper bound to the increase of interstitial pressure for porous media subjected to a homogeneous elevation of temperature assuming that the undrained boundary condition is the worst case.

Although the anisothermal theory becomes relatively well-known, only few closed-form solutions are available. Booker and Savidou [14] established an exact solution for the consolidation of the soil around a point heat source and proposed an approximate solution for a cylindrical source. McTigue [15] presented resolution methods and established exact solutions for a half-space submitted to a constant surface temperature or heat flux with either drained or undrained boundary conditions. He also derived a closed-form solution for a heated cylindrical wellbore. The case of a heat source (spherical or cylindrical) which decreases exponentially with time was treated by Giraud [16] by considering a low permeability clay for nuclear waste disposal. Wang and Papamichos [2] discussed solutions for a cylindrical wellbore and a spherical cavity subjected to a constant temperature change and heat flow rate.

This relative lack of interest during the last years for exact solutions can be explained by the development of computer simulations that permit the scientists to model complex situations. Closed-form solutions are obtained from a full linearization of the governing equations. Thus they do not account for phenomena that may be significant in many of the above-mentioned engineering fields. However, finite element analyses in poromechanics are not as 'easy' as in solid mechanics. For example, Vermeer and Verruijt [17] established that the time step is linked to the spatial discretization in a transient consolidation analysis. This phenomenon is also observed in a transient thermal analysis [18]. This problem can make the simulation of coupled mass fluid flow and heat transfer impossible for very different diffusivities. To by-pass the difficulties posed by the finite element formulation in poromechanics, Dureisseix et al. [19] have proposed a new numerical strategy.

Under these circumstances, the derivation of an exact solution for a simplified problem presents several advantages: first, it allows one to quickly obtain the prevalent material parameters for a given analysis; second, the study of this solution helps to better understand and quantify the influence of these parameters; third, it permits one to distinguish phenomena that are the consequence of the loading from those that are due to the material behavior.

This work is close to McTigue's paper [15] and complementary. McTigue has treated the case of a half-space with a homogeneous initial temperature which is submitted to a constant

temperature on its face. He has shown that the maximum interstitial pressure is constant and that the peak propagates in the half-space with a kinetics driven by the square root of time [15]. In the present study, a harmonic thermal loading is considered and the framework of the thermodynamics of open porous continuum media proposed by Coussy [20] is adopted. In the following section, the governing three-dimensional equations are summarized in their simplest form. These equations, re-written in a unidimensional setting, enable us to obtain a diffusion equation for the fluid pressure with a temperature-dependent source term. This pressure diffusion equation allows us to obtain the prevalent parameters. In the next section, a closed-form solution for a thermo-poro-elastic half-space submitted to a cyclic thermal loading is developed. The location of the maximum fluid pressure is derived and it is shown that it is related to the diffusivity ratio and the frequency of the thermal loading. Furthermore, it also shown that the maximum fluid pressure depends only on the diffusivity ratio and the thermal amplitude.

2. GOVERNING EQUATIONS AND CHARACTERISTIC PARAMETERS

The porous medium is assumed to be made of a solid continuum skeleton filled by a continuum fluid phase. The modeling is carried out in the framework of physical linearization and infinitesimal transformations. The derivation starts from the linearized equations of isotropic thermoporoelasticity [20]. The set of conservation laws includes the momentum balance for the medium, the fluid mass balance and the energy balance equations.

When inertia and body forces are neglected, the momentum balance equation is given by

$$\underline{\underline{div}}(\underline{\underline{\sigma}}) = \underline{0} \text{ in } \Omega \tag{1}$$

where $\underline{\underline{\sigma}}$ is the Cauchy stress tensor and Ω the considered volume; $\underline{\underline{\sigma}}$ a symmetric tensor because it satisfies the balance of moment of momentum equation.

By considering Darcy's law, the linearized equation for the fluid mass balance can be written as

$$\frac{1}{\rho_f}\frac{\partial m}{\partial t} = k\Delta(p - p_i) \text{ in } \Omega \tag{2}$$

where m is the variation in fluid mass content per unit initial volume, ρ_f the fluid density, k the hydraulic conductivity (by analogy to thermal conductivity), and p the fluid pressure. The subscript i denotes the initial state of any considered field. The hydraulic conductivity k is equal to the intrinsic permeability divided by the dynamic viscosity of the fluid. Equation (2) is a reduced form because the Soret effect (i.e., fluid flux due to temperature gradient) is neglected.

The energy balance equation is expressed as

$$D_T\Delta(T - T_i) = \frac{\partial T}{\partial t} \text{ in } \Omega \tag{3}$$

where T is the temperature and D_T is the thermal diffusivity of the whole medium. The convective heat transport by the pore fluid and the source terms due to the thermoelastic coupling are neglected. The Dufour effect (i.e., heat flux due to pressure gradient) is also neglected so that the heat diffusion equation is totally uncoupled when the thermal diffusivity does not depend on mechanical variables. Consequently, D_T can be regarded as an empirical

coefficient.

Equations (1)-(3) are not sufficient to determine the four unknowns. Closure is provided by the constitutive equations for the skeleton and the fluid. In this study, the skeleton is assumed to be homogeneous, isotropic and thermoelastic. All material parameters are assumed to be independent of the temperature.

The constitutive equation for the skeleton is given by [20]

$$\underline{\underline{\sigma}} = \underline{\underline{\sigma}}_i + \lambda \left(Tr\underline{\underline{\varepsilon}}\right) .\underline{\underline{I}} + 2\mu\underline{\underline{\varepsilon}} - b(p - p_i)\underline{\underline{I}} - 3\alpha_o K_o(T - T_i)\underline{\underline{I}} \tag{4}$$

with

$$b = 1 - \frac{K_o}{K_s} \tag{5}$$

where $\underline{\underline{\varepsilon}}$ is the infinitesimal strain tensor and $\underline{\underline{I}}$ the identity tensor, λ and μ Lamé's coefficients, α_o the drained coefficient of thermal expansion, K_o the compressibility of the saturated porous medium in drained conditions, K_s the compressibility of the skeleton and b Biot's coefficient ($b = 1$ for both skeleton and fluid incompressibility).

The constitutive equation for the fluid is expressed as [20]

$$p = p_i + M\,(-bTr\underline{\underline{\varepsilon}} + \frac{m}{\rho_f}) + 3\alpha_m M\,(T - T_i) \tag{6}$$

with

$$\alpha_m = (b - 1)\alpha_0 + (1 - \Phi_i)\alpha_s + \alpha_f \Phi_i \tag{7}$$

and

$$\frac{1}{M} = \frac{b - \Phi_i}{K_s} + \frac{\Phi_i}{K_{fl}} \tag{8}$$

where α_s and α_f are the coefficients of thermal expansion of the skeleton and fluid, respectively, Φ the porosity, K_{fl} the compressibility of the fluid and M Biot's modulus depending on porosity, skeleton and fluid compressibility ($M \to \infty$ for both fluid and skeleton incompressibility).

This set of equations [(1),(2),(3),(4),(6)] is completed by a set of initial and boundary conditions depending on the considered problem. It is not necessary to specify them to obtain the parameters that control the pressure fluctuations due to thermal loading.

2.1. One-dimensional pressure diffusion equation

To identify the characteristic parameters, let us consider a saturated porous medium subjected to a one-dimensional heat flux, in combination with a plane strain state. Therefore, the displacement is given by $\underline{u}(M,t) = u(x,t)\underline{e}_x$. In this case, by using the constitutive equation (4), the momentum balance equation (1) leads to a one-dimensional Navier's equation

$$\frac{\partial}{\partial x}\left[a\frac{\partial u}{\partial x} - \frac{b}{3K_0}P - \alpha_0\theta\right] = 0 \tag{9}$$

with

$$a = \frac{1 - \nu_0}{1 + \nu_0} \tag{10}$$

where ν_o is the drained Poisson's ratio, $P = p - p_i$ and $\theta = T - T_i$ the change of fluid pressure and temperature, respectively. Similarly, by using the constitutive equation (6), the fluid mass balance equation (2), one obains

$$\frac{\partial^2 P}{\partial x^2} - \frac{1}{kM}\frac{\partial P}{\partial t} = \frac{b}{k}\frac{\partial^2 u}{\partial x \partial t} - \frac{3\alpha_m}{k}\frac{\partial \theta}{\partial t} \,. \tag{11}$$

The heat diffusion equation (3) is expressed as

$$\frac{\partial^2 \theta}{\partial x^2} - \frac{1}{D_T}\frac{\partial \theta}{\partial t} = 0 \ : . \tag{12}$$

To establish a relationship between the temperature and the fluid pressure, Eqs. (9) and (11) are recast to remove the displacement. For problems involving a traction-free surface (at $x = 0$), the integration of Eq. (9) over x yields

$$a\frac{\partial u}{\partial x} = \alpha_0 \theta + \frac{b}{3K_0} P \,. \tag{13}$$

Substituting Eq. (13) into Eq. (11) and using Eq. (12) leads to

$$\frac{\partial^2 P}{\partial x^2} - \frac{1}{D_H}\frac{\partial P}{\partial t} = \frac{\delta_v D_T}{k}\frac{\partial^2 \theta}{\partial x^2} \tag{14}$$

where D_H is the hydraulic diffusivity (by analogy to the thermal diffusivity) and is defined by

$$D_H = k\left(\frac{1}{M} + \frac{b^2}{3aK_0}\right)^{-1} \tag{15}$$

and δ_v the coefficient of relative bulk variation

$$\delta_v = \frac{b}{a}\alpha_0 - 3\alpha_m \,. \tag{16}$$

This result is in agreement with that of McTigue [15]. The fluid pressure P is governed by a pressure diffusion equation with a source term depending on the temperature field. Equation (14) and the heat diffusion equation (12) constitute a convenient set to study the transient pore pressure response to a thermal loading. Since the heat diffusion equation is uncoupled, the temperature can be seen as a bulk load for the pressure diffusion equation.

2.2. Characteristic parameters

Equation (15) shows that the hydraulic diffusivity D_H is related to the intrinsic permeability (equal to the hydraulic conductivity multiplied by the dynamic viscosity of the fluid) and the relative bulk compressibility of both the fluid and the solid skeleton (i.e., influence of the Biot's modulus M). Consequently, a high intrinsic permeability does not necessarily produce a high hydraulic diffusivity.

The diffusivity ratio $\frac{D_H}{D_T}$ has a strong influence on the excess of the pore pressure level induced by thermal loading. If the hydraulic diffusivity is significantly greater than the thermal diffusivity, the bulk variation pore/fluid due to the thermal loading can easily be accommodated by the rapid motion of fluid. The pressure remains almost constant and equal

to the initial value. Conversely, the pressure increases to a maximum and then levels off due to the fluid motion.

Equation (16) with Eq. (7) yields

$$\delta_v = \alpha_0 \left[b(\frac{1}{a} - 3) + 3 \right] - 3 \left[(1 - \Phi)\alpha_s + \Phi\alpha_f \right] . \tag{17}$$

This expression for the coefficient of relative bulk variation δ_v shows that there exist two sources of bulk variation: namely, the differential pore/fluid expansion and the poroelastic coupling. By noting that the drained coefficient of thermal expansion α_0 must be less than or equal to that of the skeleton α_s, Eq. (17) can be rewritten as

$$\delta_v \leq 3 \left[\alpha_s \left(\Phi + b \left(\frac{1}{3a} - 1 \right) \right) - \Phi\alpha_l \right] . \tag{18}$$

Biot's coefficient b is always less than or equal to unity [20] and the drained Poisson's ratio ν_o is less than 0.5, therefore a is greater than $\frac{1}{3}$. An upper bound for δ_v can be proposed

$$\delta_v \leq 3\Phi \left(\alpha_s - \alpha_l \right) . \tag{19}$$

In general, the coefficient of thermal expansion of solids is less than that of liquids. This can be justified by the stronger atomic bonds in solids. Consequently, the coefficient of relative bulk variation δ_v is negative. This result, in conjunction with the pressure diffusion equation (14), shows that the pressure increases with temperature. Because δ_v is negative, the source term of Eq. (14) is proportional to the opposite of the curvature of the temperature difference *theta*.

The coefficient δ_v has also a direct influence on the maximum pressure induced by a temperature increase. For example, in the case of undrained conditions, assuming that $m = 0$ in the pore pressure constitutive equation (6) leads to

$$P = M \left(3\alpha_m \theta - b \frac{\partial u}{\partial x} \right) . \tag{20}$$

The substitution of Eq. (20) into Eq. (13) provides the link between the pressure in undrained conditions P_{nd} and the temperature change θ

$$P_{nd} = -\delta_v \left(\frac{1}{M} + \frac{b^2}{3aK_0} \right)^{-1} \theta . \tag{21}$$

This undrained pressure is the maximum interstitial pressure reached for a homogenous thermal loading [13]. For heterogeneous heating, if one replaces the value of θ by the maximum change in temperature θ_{max}, it is reasonable to consider P_{nd} as an upper bound. However, as it will be shown below, it is possible to exceed this value. It is expected that P_{nd} remains close to the maximum, and it can be considered as a characteristics of the problem. Furthermore, this expression shows clearly the influence of δ_v on the maximum interstitial pressure.

3. CYCLIC HEATING OF A HALF-SPACE

To establish a solution for Eq. (14) to obtain the prevalent parameters and examine their influence on the pressure fluctuation induced by a cyclic thermal loading, additional hypotheses

are necessary. First, let us consider a half-space domain with a traction-free surface. The traction-free surface corresponds to the origin of the x axis. Second, let us assume that the fluid pressure variation P at the x axis origin remains equal to zero during loading (e.g., drained boundary condition). Third, let us consider a harmonic temperature variation prescribed on the surface of the half-space (i.e., $x = 0$). Consequently, it is possible to write

$$\theta(x = 0, t) = \frac{\Delta T}{2} cos(wt + \phi) \tag{22}$$

where w is the frequency of the cyclic loading, ΔT its amplitude and ϕ a phase lag. Under these hypotheses, since the heat diffusion equation (12) is uncoupled when the steady-state regime is considered, the solution is expressed as [21]

$$\theta(x, t) = \frac{\Delta T}{2} cos(wt - K_T x + \phi) e^{-K_T x} \tag{23}$$

with

$$K_T = \sqrt{\frac{w}{2D_T}} \tag{24}$$

where K_T is the wave number of the heat propagation. Equation (23) describes a wave propagation with a forced time oscillation and a spacial damping (Fig. 1).

[Figure 1 about here.]

Solution (23) is considered as a loading for the pressure diffusion equation (14). By using a classical calculation [21], the solution of (14) is obtained for $D_H \neq D_T$ (see Appendix A)

$$P(x, t) = \beta \left(e^{-K_T x} cos(wt - K_T x + \phi) - e^{-K_H x} cos(wt - K_H x + \phi) \right) \tag{25}$$

with

$$\beta = \frac{\delta_v}{k} \frac{D_T D_H}{D_H - D_T} \frac{\Delta T}{2} \tag{26}$$

and

$$K_H = \sqrt{\frac{w}{2D_H}} \tag{27}$$

where K_H is the wave number of the fluid mass flow, considering a harmonic pressure loading at the traction-free surface in combination with isothermal conditions. Equation (25) characterizes the propagation of a pressure wave with a time forced oscillation and a spatial damping (Fig. 2). The pressure is induced by the competition between heat and fluid mass propagation. Equation (26) shows that the parameter β is singular when $D_H = D_T$. However, Eq. (25) can be extended by continuity (Appendix B). As shown in Fig. 2, the absolute maximum pressure P_{max} is reached behind the traction-free surface for an abscissa x_{cr}.

[Figure 2 about here.]

3.1. Location of the maximum pressure

Let us now determine the abscissa x_{cr} of the absolute maximum pressure P_{max}. It is essential to know the expression for x_{cr} to establish that of P_{max}. In addition, it allows us to understand how the loading influences the maximum pressure location.

Equation (25) is transposed in the complex space. The associated complex function $\tilde{P}(x,t)$ reads

$$\tilde{P}(x,t) = \beta \tilde{F}(x)\ e^{i(wt+\phi)} \tag{28}$$

with

$$\tilde{F}(x) = e^{-(1+i)K_T x} - e^{-(1+i)K_H x} \tag{29}$$

One can observe that $\tilde{P}$ is the product of two complex functions: one has a unit modulus and a time dependent phase (i.e., the term $e^{i(wt+\phi)}$) and the second one has modulus and phase that depend on x (i.e., the term $\tilde{F}$). Because of this feature, the pressure fluctuation amplitude is only dependent on the abscissa and the local maximum pressure is not reached simultaneously at each point because of the phase lag. Since $P(x,t)$ is the real part of the complex function, it can also be written as

$$P(x,t) = |\beta|.||\tilde{F}(x)|| \cos(wt + \psi(x)) \tag{30}$$

The term $|\beta|.||\tilde{F}(x)||$ is the maximum pressure fluctuation at each point. To find the maximum of $P(x,t)$ one can maximize the modulus of $\tilde{F}$. Therefore, x_{cr} must satisfy

$$\frac{d}{dx}||\tilde{F}(x)|| = 0 \tag{31}$$

With the assumption that $||\tilde{F}(x_{cr})|| \neq 0$ (reasonable for a maximum), x_{cr} is solution to the following equation

$$e^{-\gamma x} + \mu e^{\gamma x} = (1+\mu)\cos(\gamma x) + (1-\mu)\sin(\gamma x) \tag{32}$$

with

$$\gamma = K_T - K_H = \sqrt{\frac{w}{2}}\ \left[\frac{1}{\sqrt{D_T}} - \frac{1}{\sqrt{D_H}}\right] \tag{33}$$

and

$$\mu = \frac{K_H}{K_T} = \sqrt{\frac{D_T}{D_H}} \tag{34}$$

where μ is a material-dependent parameter. It is characteristic of the relative kinetics of the heat diffusion and fluid mass transfer. The constant γ depends on both material and loading parameters. It is due to the phase lag between the thermal and hydraulic waves and is strongly related to the kinetics of the loading, described by the frequency w.

The abscissa of each local maximum of $||\tilde{F}(x)||$ is the solution to Eq. (32). The trivial solution $x_{cr} = 0$ is not in agreement with the hypothesis $||\tilde{F}(x_{cr})|| \neq 0$ made to obtain Eq. (32). Furthermore, x_{cr} is the abscissa of the absolute maximum and an upper bound of $P(x,t)$ is a sum of decreasing exponentials (see Eq. (25)). Consequently, x_{cr} is the lowest strictly positive solution to Eq. (32). To our knowledge, a closed-form solution to this equation does not exist. Approximate solutions are now proposed to analyze the influence of the prevalent parameters.

3.1.1. Similar diffusivities. Let us examine the case when D_H and D_T have the same order of magnitude, but are not equal. A first order approximation yields

$$\mu \simeq 1 \tag{35}$$

Cosine and sine functions are less than unity, thus the solution to Eq. (32) must be the sum of exponentials less than 2. Consequently, the product γx_{cr} must to be less than unity. Equation (32) can be approximated by

$$e^{-\gamma x} + e^{\gamma x} = 2\cos(\gamma x) \tag{36}$$

We can conclude that the solution x_{cr} of Eq. (32) is such that $\gamma x_{cr} \simeq 0$. Consequently, Eq. (32) can be simplified

$$e^{\gamma x}\left(e^{-\gamma x} - \mu\right)\left(e^{-\gamma x} - 1\right) = 0 \tag{37}$$

The only non zero solution is given by

$$x_{cr} = \frac{-1}{\gamma}\ln(\mu) = \sqrt{\frac{2D_T}{w}}\frac{1}{\mu - 1}\ln(\mu) \tag{38}$$

One can note that $\gamma x_{cr} = -\ln(\mu)$, which is in agreement with the assumption made previously. The product γx_{cr} is as close to zero as μ is close to one.

3.1.2. Very different diffusivities. Two cases must be examined: namely, K_T much greater than K_H, and the inverse case. First, let us assume that K_T is much greater than K_H (i.e., $\mu \ll 1$). By considering a first order approximation, one has

$$\mu \simeq 0 \quad \text{and} \quad \gamma \simeq K_T \tag{39}$$

Equation (32) can be approximated by

$$e^{-\gamma x} + \mu e^{\gamma x} = \cos(\gamma x) + \sin(\gamma x) \tag{40}$$

To our knowledge, this equation does not admit a closed-form solution. A graphical resolution is proposed: let δ be equal to γx, Fig. 3 shows the change of the functions involved in Eq. (40) with δ for different values of μ.

[Figure 3 about here.]

Let us assume that δ is close to 0, then, as a first order approximation, accounting for the expression (24) for γ, Eq. (32) can be rewritten as

$$-K_T(1-\mu)^2 x = K_T(1-\mu)^2 x\,. \tag{41}$$

The solution $x = 0$ has been previously rejected. Consequently, δ close to zero imposes that μ be close to one. The solution for Eq. (41), which tends to $\delta = 0$, is not valid as a solution to Eq. (32) when $\mu \ll 1$.

The other solution δ_{cr} to Eq. (40) tends quickly to $\frac{3\pi}{4}$ when μ decreases. A Taylor expansion of Eq. (40) about $\frac{3\pi}{4}$ yields

$$e^{-\frac{3\pi}{4}} + \mu e^{\frac{3\pi}{4}} + \left(\delta - \frac{3\pi}{4}\right)\left(-e^{-\frac{3\pi}{4}} + \mu e^{\frac{3\pi}{4}}\right) = -\sqrt{2}\left(\delta - \frac{3\pi}{4}\right)\,. \tag{42}$$

The solution is then given by

$$x_{cr} \simeq \sqrt{\frac{2D_T}{w}}\, f(\mu) \tag{43}$$

with

$$f(\mu) = \frac{3\pi}{4} - \frac{e^{-\frac{3\pi}{4}} + \mu e^{\frac{3\pi}{4}}}{\sqrt{2} - e^{-\frac{3\pi}{4}} + \mu e^{\frac{3\pi}{4}}} \tag{44}$$

Second, when K_T is much less than K_H (i.e., $\mu \gg 1$), Eq. (32) can be written in the same way as (40) where μ and γ are replaced by μ' and γ' where $\mu' = \frac{1}{\mu}$ and $\gamma' = K_H$. Thus, the abscissa x_{cr} is found to be

$$x_{cr} \simeq \sqrt{\frac{2D_H}{w}}\, f\left(\frac{1}{\mu}\right) \tag{45}$$

3.1.3. Comments on the location of P_{max}. A good agreement between the explicit approximate solutions of x_{cr} established previously and that obtained by numerical resolution of Eq. (32) with Matlab 5.2. [22] is shown in Fig. 4. To compare numerical results and our estimations, it is convenient to use the dimensionless abscissa $K_T x_{cr}$. By using Eqs. (38), (43) and (45) for x_{cr}, this dimensionless abscissa only depends on μ. In Fig. 4, the approximate solutions are given by Eqs. (43) for μ varying between 0 and 0.7, (38) for μ ranging from 0.7 to 3, and (45) for μ varying between 3 and 1000.

[Figure 4 about here.]

One can note that Eqs. (38), (43) and (45) are proportional to the inverse of the square root of the frequency for a given diffusivity ratio. It appears that the location x_{cr} of the maximum interstitial pressure P_{max} is directly influenced by the frequency of the thermal loading: the higher the frequency, the lower x_{cr}. The influence of the frequency w and the diffusivity ratio on the abscissa x_{cr} is shown in Fig. 5.

[Figure 5 about here.]

3.2. Maximum pressure

Let us now substitute the definition of the hydraulic diffusivity D_H (15) in the expression of the pressure in undrained conditions P_{nd} (21) and replace θ by $\frac{\Delta T}{2}$. It yields

$$P_{nd} = -\frac{\delta_v D_H}{k}\frac{\Delta T}{2} \tag{46}$$

Equation (26) defining β can be rewritten as

$$\beta = -\frac{D_T P_{nd}}{D_H - D_T} \tag{47}$$

By accounting for the definitions (33) and (34) for γ and μ, and substituting them in the expression of the modulus of $\tilde{F}$ (29) and using Eq. (47), for each location x, the maximum pressure is given by

$$\frac{P_{max}(x)}{P_{nd}} = \left|\frac{\mu^2}{1-\mu^2}\right| \sqrt{1 + e^{-2\gamma x} - 2e^{-\gamma x} cos(\gamma x)} \quad e^{-K_H x} \tag{48}$$

The maximum pressure in the medium is defined by

$$P_{max} = \sup_{x \in]0,\infty[} (P_{max}(x)) \tag{49}$$

By definition, this maximum pressure is located at $x = x_{cr}$. By noting that the product γx_{cr} in Eq. (48) does not depend on w, the dimensionless maximum pressure only depends on the diffusivity ratio

$$\frac{P_{max}}{P_{nd}} = g(\mu) \tag{50}$$

where $g(\mu)$ is a function defined over different ranges of μ:

- When $\mu \simeq 1$, substituting Eq. (38) for x_{cr} into Eq. (48) yields

$$\frac{P_{max}}{P_{nd}} = \left|\frac{\mu^2}{1-\mu^2}\right| \sqrt{1+\mu^2-2\mu\cos[Ln(\mu)]} \quad \mu^{\frac{\mu}{1-\mu}} \tag{51}$$

- When $\mu < 0.7$, substituting Eq. (43) for x_{cr} into Eq. (48) yields

$$\frac{P_{max}}{P_{nd}} = \left|\frac{\mu^2}{1-\mu^2}\right| \sqrt{1+e^{-2(1-\mu)f(\mu)}-2e^{-(1-\mu)f(\mu)}\cos[(1-\mu)f(\mu)]} \quad e^{-\mu f(\mu)} \tag{52}$$

- When $\mu > 3$, substituting Eq. (45) for x_{cr} into Eq. (48) yields

$$\frac{P_{max}}{P_{nd}} = \left|\frac{\mu^2}{1-\mu^2}\right| \sqrt{1+e^{-2(\frac{1}{\mu}-1)f(\frac{1}{\mu})}-2e^{-(\frac{1}{\mu}-1)f(\frac{1}{\mu})}\cos[(\frac{1}{\mu}-1)f(\frac{1}{\mu})]} \quad e^{-f(\frac{1}{\mu})} \tag{53}$$

These three equations define the solid line drawn in Fig. 6. The points correspond to Eq. (48) for which x_{cr} is obtained by numerical resolution of Eq. (32) with Matlab 5.2. [22]. A good agreement is obtained between the the two predictions.

[Figure 6 about here.]

3.2.1. Comments. These results allow us to calculate in a simple way the maximum interstitial pressure reached for a given load. Moreover, Eq. (46) of the undrained pressure P_{nd} shows that the range of pressure fluctuation is only dependent on the range of the thermal loading.

One can note in Fig. 6 that, for low diffusivity ratios, the maximum pressure P_{max} is greater than the undrained pressure P_{nd}. The dimensionless pressure tends to 1.07. This value, greater than one, is not due to numerical approximations for the resolution or to the first order approximations. The maximum pressure indeed exceeds the undrained reference. By substituting Eq. (13) into the constitutive equation for the fluid pressure (6) yields

$$\frac{m}{\rho_f} = \left(\frac{1}{M} + \frac{b^2}{3aK_o}\right) P + \left(\frac{\alpha_o b}{a} - 3\alpha_m\right)\theta \tag{54}$$

By recasting Eq. (54) and accounting for Eqs. (46) for P_{nd}, (15) for D_H and (16) for δ_v yields at $x = x_{cr}$

$$\frac{m}{\rho_f}(x_{cr}, t_{cr}) = \delta_v \left(\theta_{cr} - \frac{\Delta T}{2}\frac{P_{max}}{P_{nd}}\right) \tag{55}$$

It is worth remembering that δ_v is negative and

$$\theta_{cr} < \frac{\Delta T}{2} \tag{56}$$

Since δ_v is negative and θ_{cr} is less than $\frac{\Delta T}{2}$, the change in fluid mass content $m(x_{cr}, t_{cr})$ is positive. Consequently, the 'overpressure' can be explained by a positive change in fluid mass content coupled with a negative relative bulk variation. This condition is even more severe than the classical undrained boundary condition (i.e., $m = 0$).

This result can also be explained from a physical point of view. The range of temperature fluctuation is not the same at each point and there exists a spacial phase lag. Therefore, the volume fluctuation is not homogeneous, and the fluid mass flow too. Furthermore, to verify the fluid mass balance, the change in fluid mass content m cannot be negative at each point. Consequently, the fluid mass flow is one dimensional but not with the same direction at all points at a given time. It is possible to visualize schematically what is happening: let us imagine three elementary volumes, totally filled with liquid, connected in only one direction and drained on the two boundaries. When submitting them to a rapid heterogeneous heating, the temperature variation is the highest on the boundary volumes. Due to their contraction, the three volumes expel their excess in fluid. Therefore, the volume in the middle tries to expel its excess volume but, in the same time, it receives the fluid mass flow from its two neighbors. Therefore, the pressure can exceed the undrained reference.

Conversly, for single heating of a half space, the heat and fluid mass flow are always in the same direction, and the master curve (Fig. 6) gives an upper bound to the pressure. By using McTigue's work [15], it is possible to draw the curve that relates the dimensionless maximum pressure to the diffusivity ratio for a constant temperature prescribed on the surface of a semi-infinite saturated porous medium with an initial homogeneous temperature. The two curves are compared in Fig. 7. One can see that the maximum pressure induced by a Heaviside temperature applied on the traction-free surface is less than that generated by a harmonic thermal history.

[Figure 7 about here.]

4. EXTENSION TO A FINITE MEDIUM AND FOR OTHER BOUNDARY CONDITIONS

4.1. Validity of the results for a finite medium

For a one-dimensional problem of a finite medium, it is reasonable to model it by a semi-infinite medium if its thickness is greater than the wave length λ defined by [21]

$$\lambda = \frac{2\pi}{K} \tag{57}$$

where K is the wave number. By using Eqs. (24) for K_T and (27) for K_H, the previous results are still valid for finite media of thickness t when

$$t > 2\pi\sqrt{\frac{2}{\omega}}\ \sup\left(\sqrt{D_H}, \sqrt{D_T}\right)\ . \tag{58}$$

The higher the frequency of the thermal load, the thinner the considered wall can be.

4.2. Other thermal boundary conditions on the traction-free surface

In the above study, only the case of a prescribed temperature on the traction-free surface has been considered. It is interesting to examine the case of a prescribed heat flux, usually

modeled by convection or radiation. A prescribed temperature gives an upper bound of the possible thermal loading. Consequently the maximum pressure derived previously is also an upper bound for the problem with a prescribed heat flux.

In the considered application (i.e., impregnation-spalling of the inner lining of a steel ladle), the problem cannot be described by a semi-infinite porous medium because the thickness of the considered wall is too thin. Therefore, the goal is to check that the master curve, which has been established for a half-space, gives an upper bound to the dimensionless maximum pressure for a wall of finite thickness. The presence of a second edge facilitates the pressure relaxation by fluid mass flow through the back face.

Numerical simulations have been performed by using the finite element code Abaqus-5.8 [23] with drained boundary conditions (i.e., $P = 0$ on the two ends) and assuming a plane strain state. First, the heat transfer computations are solved by considering a convection heat exchange on the two traction-free faces with a constant temperature in the outer medium and two different temperatures in the inner ladle, one during heating and one during cooling. Second, the space-time temperature field has been used as loading for the poroelastic computations. Many simulations have been performed to control the effect of the diffusivity ratio, the heat exchange coefficient prescribed on the thermally loaded face (inner ladle).

As could be anticipated, the maximum pressure is dependent on the diffusivity ratio and is also influenced by the thermal exchange coefficient on the hot face. Furthermore, the maximum interstitial pressure is located a few centimeters from the hot face and its location is close to that of microcracks observed in bricks [24]. Figure 8 shows that all the values of the maximum dimensionless pressure lie under the master curve. Moreover, the higher the heat exchange coefficient, the closer the simulation to the master curve that was obtained for a prescribed temperature history on the free surface.

[Figure 8 about here.]

5. CONCLUSION

In this paper, the behavior of a homogeneous, isotropic and elastic saturated open porous medium has been studied when subjected to a cyclic thermal loading on its traction-free surface. First, by using the fully linearized governing equations, we have shown that the interstitial pressure is related to the temperature field by a pressure diffusion equation with a source term that depends on the local heating (or cooling) rate. The analysis of this partial differential equation allows us to obtain a set of prevalent material parameters that affect the response of the medium, namely: the coefficient of relative bulk variation δ_v (Eq. (16)) and the diffusivity ratio μ (Eq. (34)). For a given thermal loading, the maximum interstitial pressure depends upon these parameters as well as the thermal range of the loading.

In the particular case of a semi-infinite porous medium submitted to a harmonic temperature loading on its free face, a closed-form solution for the fluid pressure is obtained by solving the pressure diffusion equation. It is shown that a pressure peak appears behind the traction free surface and the study of this solution shows that:

- the position of the maximum pressure peak mainly depends on the frequency of the load:

the higher the frequency, the closer the peak to the loaded surface.
- the maximum dimensionless pressure is related to the diffusivity ratio by a master curve (Fig. 6).

It has also been established that the pressure induced by a uniform temperature in undrained conditions P_{nd} can sometimes be exceeded. Moreover, a cyclic thermal loading is more severe compared to the Heaviside thermal loading studied by McTigue [15] in drained boundary conditions or to the homogeneous heating in undrained condition treated by Palciauskas [13]. Consequently, the master-curve (Fig. 6) defines a general upper bound for thermal loading conditions.

In summary, even if this fully linearized theory should not be applied without some caution because it is accounting for a limited phenomenology, the master-curve can be used in engineering applications to estimate quickly the maximum interstitial pressure induced by a thermal loading. Furthermore, it important to note that the undrained pressure underestimates the maximum pressure for low diffusivity ratios.

ACKNOWLEDGEMENT

This work was funded by CRDM / Sollac Dunkerque (USINOR, France). The authors wish to acknowledge stimulating discussions with Prof. J. Poirier and Dr. P. Blumenfeld.

REFERENCES

1. J.-F. Thimus, Y. Abousleiman, A.H.-D. Cheng, O. Coussy, E. Detournay (Editors) *Poromechanics, a tribute to Maurice A. Biot* A.A Balkema/Rotterdam (the Netherlands), 1998.
2. Y. Wang and E. Papamichos. Thermal effects on fluid flow and hydraulic fracturing from wellbores and cavities in low-permeability formations. *Int. J. Num. Anal. Meth. Geomech.* 1999; **23**:1819 -1834.
3. D. Gawin, C. E. Majorana and B. A. Schrefler Numerical analysis of hygro-thermal behavior and damage of concrete at high temperature *Mech. Cohes. Frict. Mater* 1999; **4**:37 - 74.
4. C. A. Kodres. Moisture induced pressures in concrete airfield pavements. *J. of Mat. Civ. Eng.* 1999; **8**(1):41-50.
5. B. Gatmiri and P. Delage. A formulation of fully coupled thermal-hydraulic-mechanical behavior of saturated porous medium: Numerical approach. *Int. J. Numer. Anal. Methods Geomech.* 1997; **21**:199-225.
6. G. W. Scherer. Thermal expansion kinetics: Method to measure permeability of cementitious materials: I, theory. *J. Am. Ceram. Soc.* 2000; **83**(11):2753-2761.
7. E. Blond, N. Schmitt, F. Hild, J. Poirier and P. Blumenfeld. Thermomechanical stresses in slag-impregnated refractories. *Proc. United International Technical Conference on Refractories* 2001; **3**:1340-48
8. M. A. Biot. General theory of three-dimensional consolidation. *J. Appl. Physics* 1941; **12**(2):151 - 161.
9. M. A. Biot. Theory of elasticity and consolidation for a porous anisotropic solid. *J. Appl. Physics* 1955; **26**(2):182 - 185.
10. M. A. Biot. Theory of deformation of a porous viscoelastic anisotropic solid. *J. Appl. Physics* 1956; **27**(5):459 - 467.
11. J. R. Rice and M. P. Cleary. Some basic stress diffusion solutions for fluid-saturated elastic porous media with compressible constituents. *Reviews of Geophys. and Space Phys.* 1976; **14**(2):227 - 241.
12. W. Derski and S. J. Kowalski. Equations of linear thermoconsolidation. *Arch. Mech.* 1979; **31**(3):303 - 316.
13. V. V. Palciauskas and P. A. Domenico. Characterization of drained and undrained responses of thermally loaded repository rocks. *Water Resources Research* 1982; **18**(2):281 - 290.
14. J. R. Booker and C. Savvidou. Consolidation around a point heat source. *Int. J. Num. Analyt. Meth. in Geomech.* 1985; **9**:173 - 184.
15. D. F. McTigue. Thermoelastic response of fluid-saturated porous rock. *J. of Geophysical Research* 1986; **91**(B9):9533 - 9542.
16. A. Giraud. Couplages Thermo-Hydro-Mécaniques dans les milieux poreux peu perméables : application aux argiles profondes *Ph.D. Thesis, Ecole Nationale des Ponts et Chaussées, Paris, France* 1993
17. P. A. Vermeer and A. Verruijt. An Accuracy Condition for Consolidation by Finite Elements. *Int. J. Num. Analyt. Methods in Geomech.* 1981; **5**:1 - 14.
18. *ABAQUS/Standard, User's Manual* Hibbitt, Karlsson & Sorensen, Inc. 1998; **I**:6.4.2-3
19. D. Dureisseix, P. Ladevèze and B. A. Schrefler. LATIN computational strategy for multiphysics problems *European Conference on Computational Mechanics* 26-29 June 2001, Cracow, Poland.
20. O. Coussy *Mechanics of porous continua* John Wiley and sons, New York (USA), 1995.
21. H. S. Carslaw and J. C. Jaeger *Conduction of heat in solids, second edition* Oxford University Press, Oxford (UK), 1959.
22. M. Mokhtari and A. Mesbah *Apprendre et maîtriser Matlab* Springer, Paris (France), 1997.
23. *ABAQUS/Standard, User's Manual* Hibbitt, Karlsson & Sorensen, Inc. 1998.
24. E. Blond, N. Schmitt, F. Hild, J. Poirier and P. Blumenfeld. Damage of slag-impregnated refractory in steel ladles, influence of interstitial pressure *7th. Conference and Exhibition of the European Ceramic Society*, sept. 9-13, Brugge, Belgium, 2001 (submitted to *Silicates Industriels*).

APPENDIX A

To solve diffusion equations such as Eqs. (12) or (14) in the case of a half-space submitted to a harmonic loading, it is convenient to rewrite the equation in the complex space and postulate the separation of variables [21]. The complex function associated to Eq. (23) is

$$\tilde{\theta} = \frac{\Delta T}{2} e^{-(1+i)K_T x} e^{i(wt+\phi)} . \tag{59}$$

Concerning $\tilde{\theta}$, let us assume that the pressure has the following form

$$\tilde{P} = \tilde{U}(x) e^{i(wt+\phi)} . \tag{60}$$

Then, Eq. (14) leads to

$$\frac{d^2\tilde{U}}{dx^2} - \frac{iw}{D_H}\tilde{U} = \frac{iw\delta_v}{k}\frac{\Delta T}{2} e^{-(1+i)K_T x} . \tag{61}$$

The function $\tilde{U}$ is the sum of the solution to Eq. (61) without second member and of a particular solution to this equation with a second member. The general solution to the equation without second member is [21]

$$\tilde{U}_{gen} = \alpha e^{-(1+i)K_H x} \tag{62}$$

where α is an unknown constant and K_H is defined by Eq. (27). Let us assume that the particular solution can be written as

$$\tilde{U}_{part} = \beta e^{-(1+i)K_T x} . \tag{63}$$

By introducing Eq. (63) in Eq. (61), assuming that $D_H \neq D_T$, one obtains Eq. (26) for the parameter β. Equation (26) shows that β is singular when $D_H = D_T$. However, Eq. (25) for $P(x,t)$ can be extended for this case by continuity (appendix B).

The drained boundary condition yields

$$\alpha = -\beta . \tag{64}$$

Consequently, the solution to Eq. (61) is given by

$$\tilde{P}(x,t) = \beta \tilde{F}(x)\ e^{i(wt+\phi)} \tag{65}$$

where $\tilde{F}$ is defined by Eq. (29). The interstitial pressure field is the real part of $\tilde{P}$ and we obtain Eq. (25).

APPENDIX B

Here, the goal is to show that Eq. (25) for $P(x,t)$ can be extend by continuity to the case $D_H = D_T$. Equation (25) can be rewritten in terms of an amplitude multiplied by a cosine (see Eq. (30)). Consequently, it is sufficient to check for the continuity of the modulus $|\beta|.||\tilde{F}(x)||$ to conclude on the validity of $P(x,t)$ in the case of equal diffusivities. By using Eq. (30), one can see that at each point, the amplitude of the pressure fluctuation is equal to the local maximum pressure. Therefore, we only have to extend Eq. (48) when $\mu = 1$ (Eq. (34)) that imposes that $\gamma = 0$ (Eq. (33)). A second order expansion of the exponential in Eq. (48) yields

$$\frac{P_{max}}{P_{nd}}(x) = \left|\frac{\mu^2}{1-\mu^2}\right| \sqrt{2} \quad |\gamma| \quad x e^{-K_H x} + \Theta(\gamma x)\,. \tag{66}$$

Substituting the definition (33) for γ in Eq. (66) and accounting for the definition (34) for μ yields

$$\frac{P_{max}}{P_{nd}}(x) = \frac{\mu^2}{1+\mu}\sqrt{2} \quad K_H x \quad e^{-K_H x} + \Theta(\gamma x)\,. \tag{67}$$

Consequently, the limit of the amplitude of the local maximum dimensionless pressure for equal diffusivities is given by

$$\lim_{\mu \to 1} \frac{P_{max}}{P_{nd}}(x) = \frac{1}{\sqrt{2}} \quad K_H x \quad e^{-K_H x}\,. \tag{68}$$

This expression shows that, for a given abscissa, the limit of the maximum dimensionless pressure when the hydraulic diffusivity tends to the thermal diffusivity is the same on the right side and on the left side. Consequently, Eqs. (48) and (25) for $P(x,t)$ can be extended by continuity to the case of equal diffusivities.

Furthermore, by accounting for Eq. (38), the following result is obtained

$$\lim_{\mu \to 1} \frac{P_{max}}{P_{nd}} = \frac{1}{e\sqrt{2}} \simeq 0.26 \tag{69}$$

This result is in agreement with the master-curve shown in Fig. 6.

List of Figures

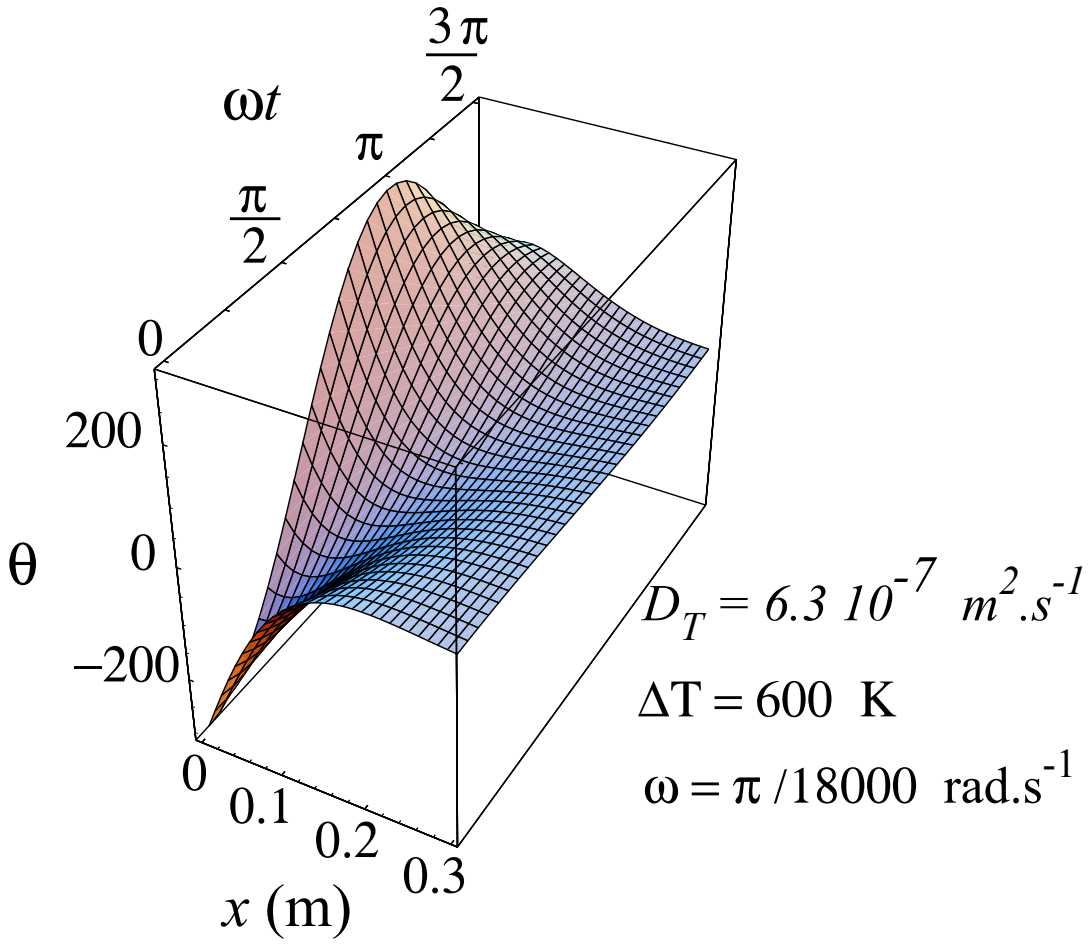

Figure 1. Temperature range versus time and space

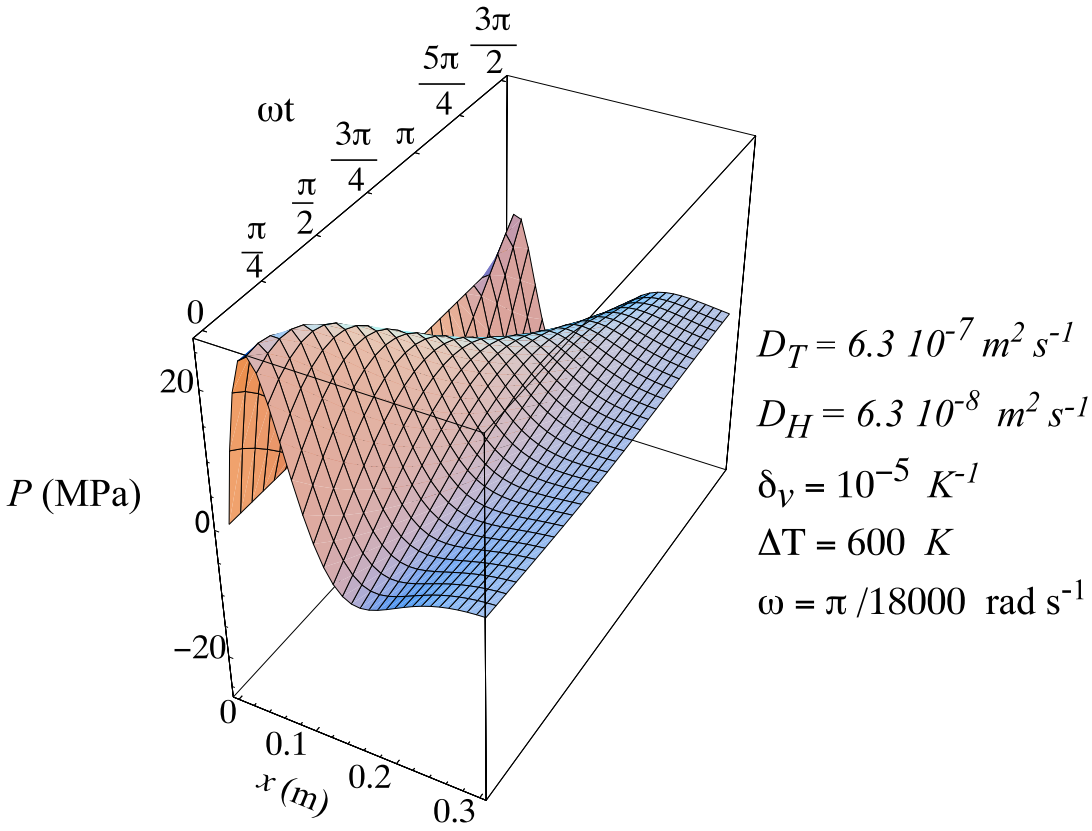

Figure 2. Interstitial pressure variation versus time and space

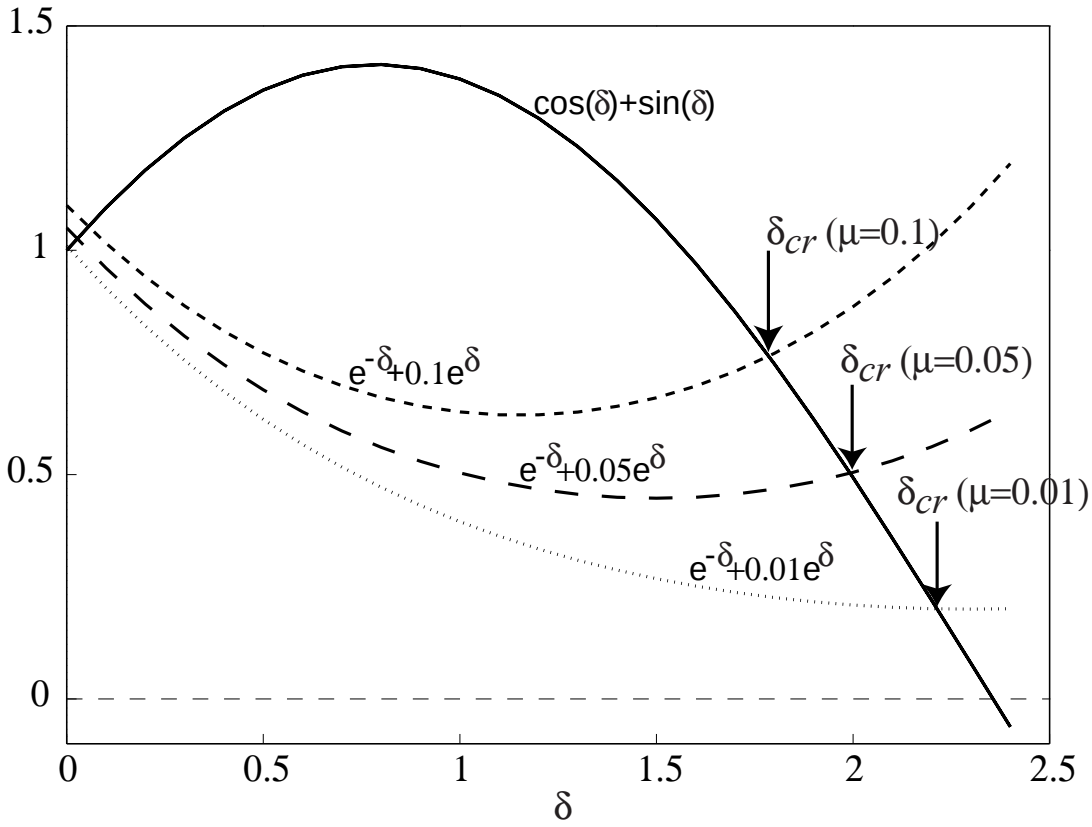

Figure 3. Graphical resolution of Eq. (40)

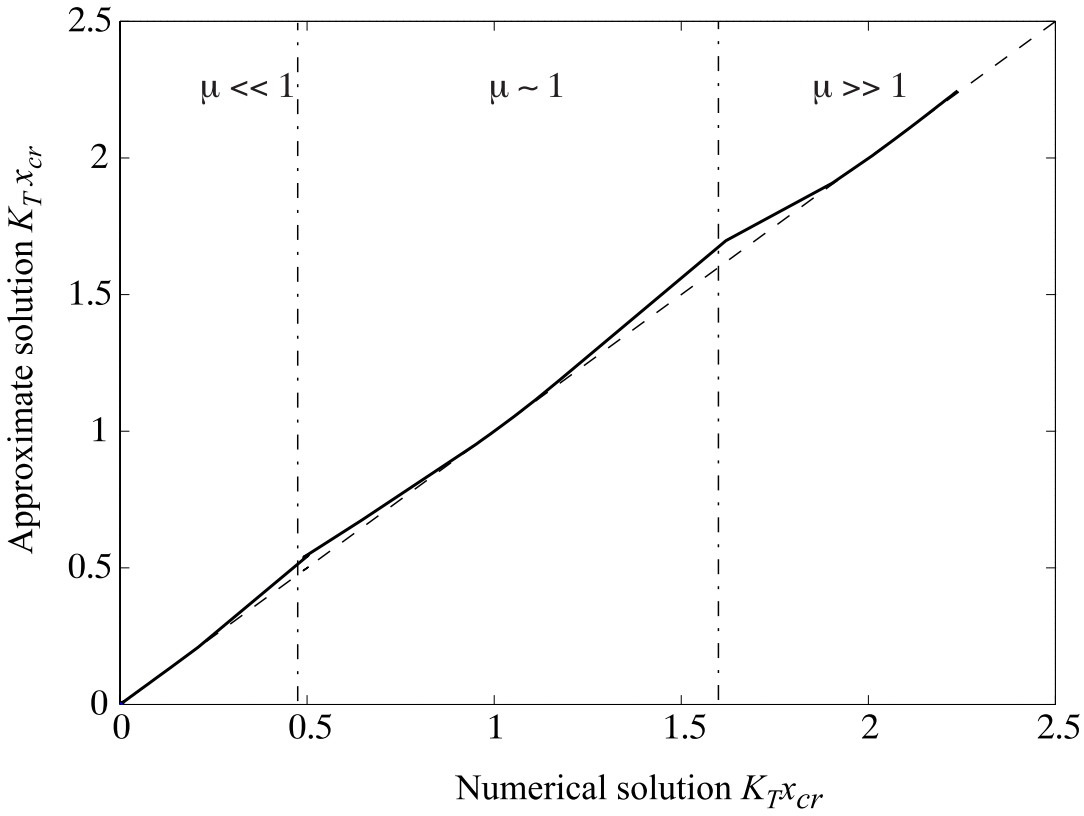

Figure 4. Comparison of Eqs. (38), (43) and (45) for x_{cr} (solid lines) with numerical solutions to Eq. (32) (dashed line)

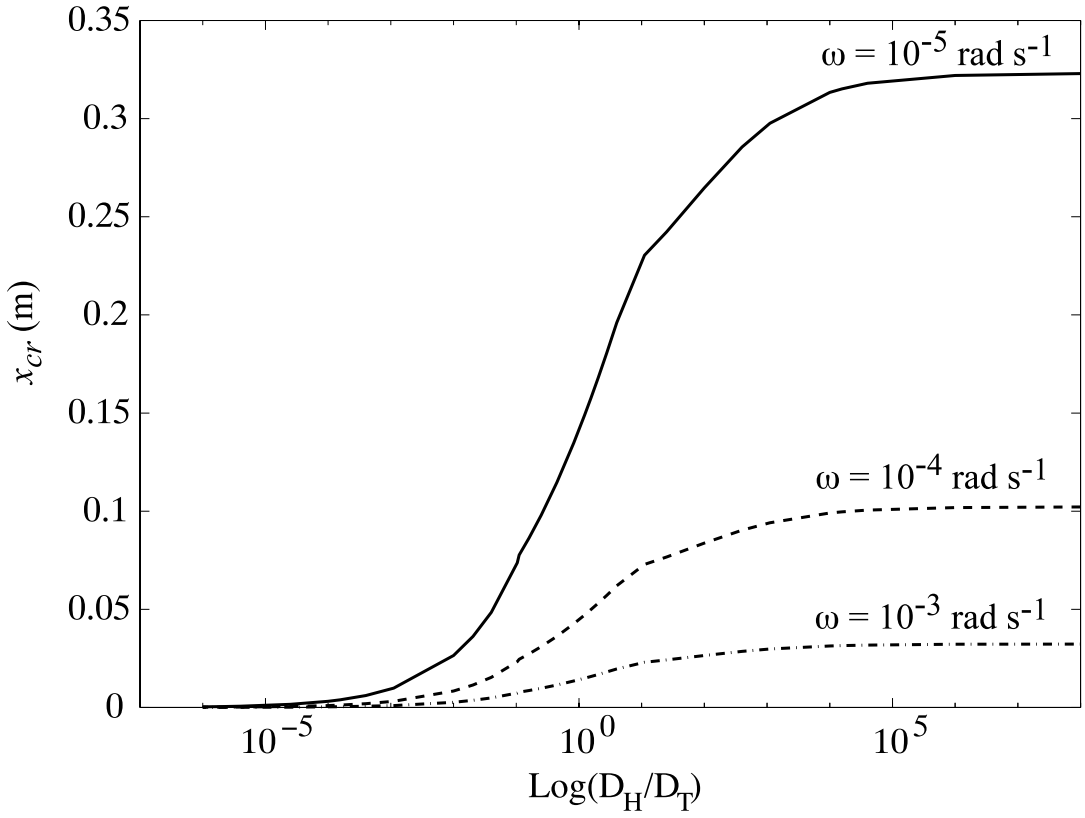

Figure 5. Influence of the frequency w and the diffusivity ratio on the abscissa x_{cr} (approximate solutions for $D_T = 10^{-7}\ m^2 s^{-1}$)

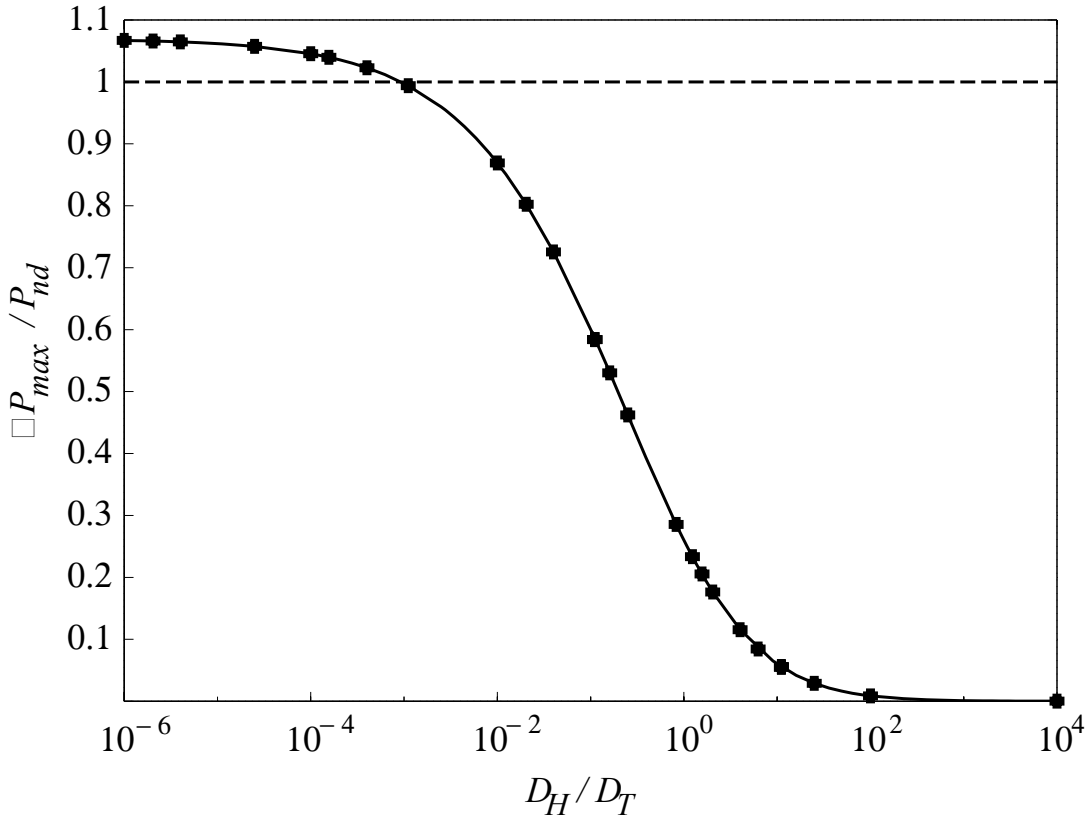

Figure 6. Maximum dimensionless pressure versus diffusivity ratio, approximate solution (solid line) and numerical solution (solid symbols)

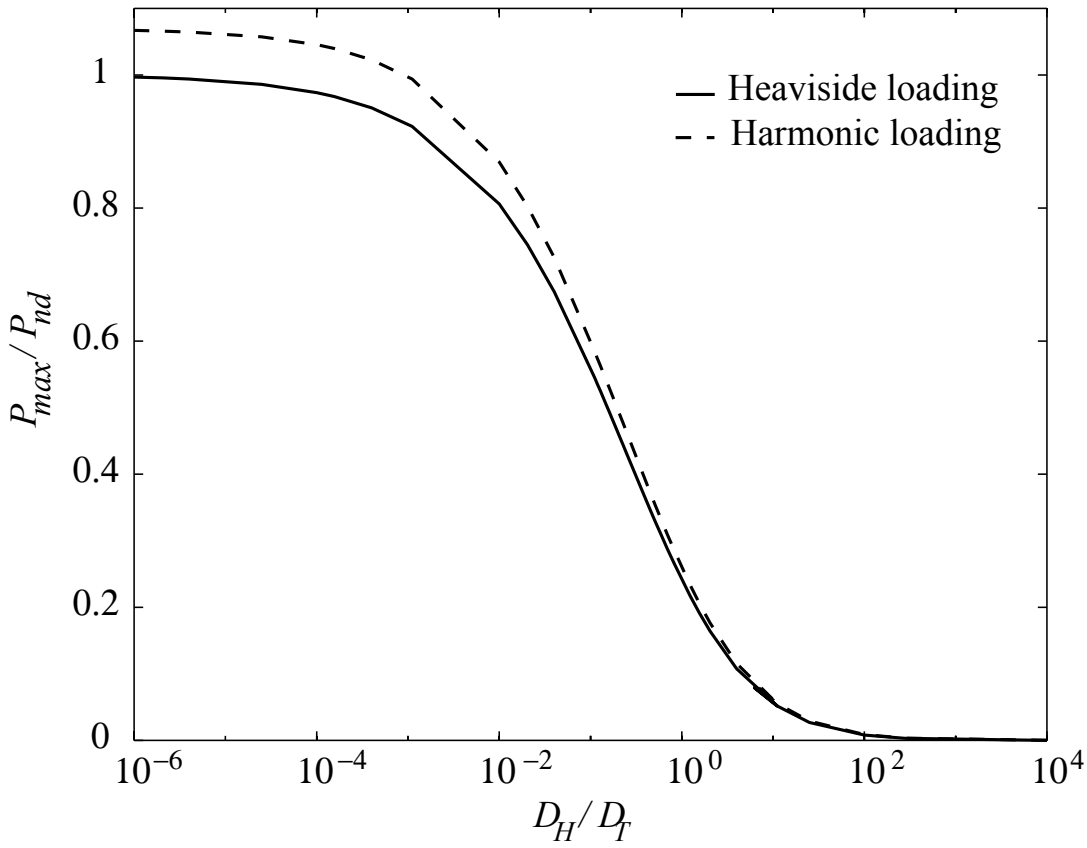

Figure 7. Maximum dimensionless pressure versus diffusivity ratio: Heaviside and harmonic loading

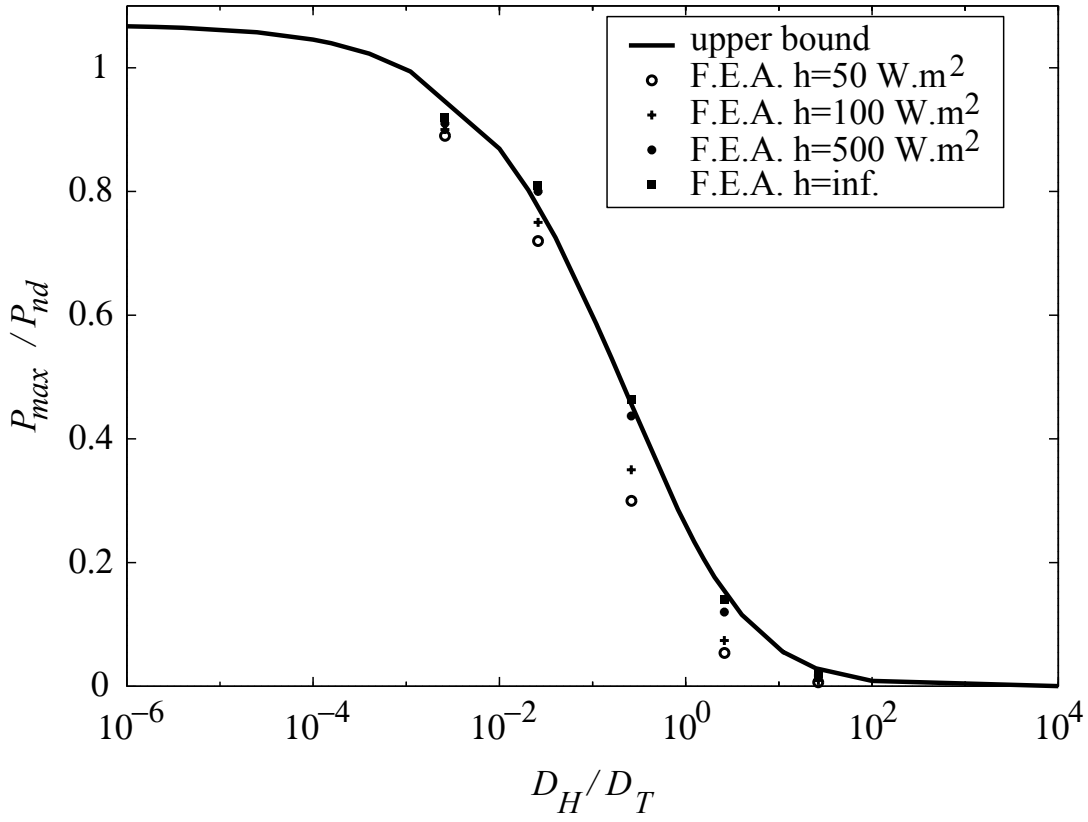

Figure 8. Maximum dimensionless pressure versus diffusivity ratio for different heat exchange coefficients, Finite Element Analysis results (symbols) and upper bound (solid line)